Journal of Alloys and Compounds 763 (2018) 289–295

Contents lists available at ScienceDirect

Journal of Alloys and Compounds

journal homepage: http://www.elsevier.com/locate/jalcom

Phase equilibria and magnetic phases in the Fe-rich regions of the Ce-Fe-{Ni, Si, Al}-B quaternary systems

Kayode Orimoloye, Dmytro Kevorkov, Mamoun Medraj*

Department of Mechanical, Industrial and Aerospace Engineering, Concordia University, 1455 de Maisonneuve Blvd. W, Montreal, Quebec, H3G 1M8, Canada

ARTICLE INFO

Article history:
Received 31 May 2017
Received in revised form
18 May 2018
Accepted 27 May 2018
Available online 29 May 2018

Keywords:
Phase equilibrium
Ce-Fe-{Ni, Si, Al}-B quaternary systems
$Ce_2Fe_{14}B$
Ce-Fe-Ni system
Magnetic phases

ABSTRACT

Fe-rich regions of the Ce-Fe-{Ni, Si, Al}-B quaternary systems were experimentally studied using diffusion couples and selected key alloys. After sufficient annealing of at least 10 days at 900 °C, samples were quenched in a cold water bath. Homogeneity ranges of $Ce_2(Fe_{14-x}Ni_x)B$, $Ce_2(Fe_{14-x}Si_x)B$ and $Ce_2(Fe_{14-x}Al_x)B$ solid solutions were measured to be ($0 \le x_{Ni} \le 1.5$), ($0 \le x_{Si} \le 2.33$) and ($0 \le x_{Al} \le 2.5$), respectively. Quaternary solid solutions $Ce(Ni_{4-x}Fe_x)B$ ($0 \le x \le 0.78$) and $(Fe_{1-x-y}Ni_xCe_y)_{23}B_6$ ($0 \le y \le 0.062$, $x = 0.832$) were also found in the Ce-Fe-Ni-B quaternary system. Except $(Fe_{1-x-y}Ni_xCe_y)_{23}B_6$, $(Fe_{1-x-y}Si_xCe_y)_{23}B_6$ and $(Fe_{1-x-y}Si_xCe_y)_3B$, all other quaternary solid solutions observed are in equilibrium with α-Fe. Magnetic force microscopy was used to screen magnetic phases. Among the phases observed in the Fe-rich regions of the Ce-Fe-{Ni, Si, Al}-B quaternary systems, only the quaternary extensions of $Ce_2Fe_{14}B$ show visible magnetic domains.

1. Introduction

Cerium is the most abundant rare earth metal, currently in market oversupply and significantly less expensive than neodymium which is used in today's most powerful permanent magnets [1]. Nevertheless, the use of Ce in permanent magnets has been discouraged due to the low Curie temperature and weaker magnetic properties in both $RE_2Fe_{14}B$ and $REFe_{12}$ compounds. Recently, magnetic hardening of $Ce_2Fe_{14}B$ by melt spinning showed potential for permanent magnet applications [2]. For the past six decades, many studies on binary and ternary systems containing rare-earths have been performed to understand the phase relationships among the phases and to obtain their crystal structures. However, higher order rare-earth containing systems have not been systematically investigated and are not well known [3]. This is essential for the quest for phase relationships among magnetic and non-magnetic phases in these multicomponent systems. In this work, we report a systematic high throughput investigation of the phase equilibria and magnetic phases in the Fe-rich regions of the Ce-Fe-{Ni, Si, Al}-B quaternary systems using diffusion couples, key alloys and magnetic force microscopy.

2. Literature review

Since the aim of this work is to experimentally investigate the Fe-rich regions of the Ce-Fe-{Ni, Si, Al}-B quaternary systems, only the four ternary systems containing Ce and Fe, out of the total ten-constituent ternary systems, will be discussed. These ternary phase diagrams are Ce-Fe-B, Ce-Fe-Al, Ce-Fe-Ni and Ce-Fe-Si.

In the Ce-Fe-B ternary system, three ternary compounds with approximate compositions of $CeFe_2B_2$, $Ce_3Fe_{16}B$ and Ce_2FeB_3 were identified [4]. No ternary solubility in the binary compounds were detected. Dub et al. [5] later identified Ce_2FeB_3 composition to have $Ce_{5-x}Fe_{2+x}B_6$ formula, but the range of "x" was not indicated in their work [5]. In a following paper, Dub et al. [6] corrected $Ce_3Fe_{16}B$ to have $Ce_2Fe_{14}B$ composition while $CeFe_2B_2$ has the $Ce_{1.1}Fe_4B_4$ composition [7,8].

Despite several experimental studies on the Ce-Fe-Al ternary system, the phase equilibria determination was only concentrated in the Al-Fe rich side. The first investigation of this system was performed as early as 1925 by Meissner [9]. However, his results were not accurate in the region less than 33.3 at.% Ce. In 1969, Zarechnyuk et al. [10] examined this ternary system with 106 alloys from 0 to 33.3 at.% Ce using X-ray diffraction (XRD) analysis. They [10] reported three ternary phases: $CeFe_2Al_{10}$, $CeFe_2Al_7$, and $CeFe_{1-1.4}Al_{1-0.6}$. They also reported that the Ce_2Fe_{17} compound dissolves up to about 60 at.% Al and that the $CeFe_2$ phase does not dissolve Al

* Corresponding author.
E-mail address: mmedraj@encs.concordia.ca (M. Medraj).

https://doi.org/10.1016/j.jallcom.2018.05.329
0925-8388/

[10]. Franceschini et al. [11] reported that Al substitutes up to 8.3 at.% Fe in $CeFe_2$, correcting the findings of Zarechnyuk et al. [10]. Zolotorevsky et al. [12] reported another ternary phase of $CeFe_4Al_8$ composition. This system has complex phase relationships in the Al-rich corner and the Ce-Fe compounds tend to dissolve significant amount of Al.

Full experimental study of the Ce-Fe-Si ternary system has been established in the literature through many isothermal sections. Bodak et al. [13] in 1970 used XRD to study the Ce-Fe-Si ternary system in the 0–33.3 at.% Ce range at 400 °C and the 33.3–100 at.% Ce range of at 800 °C. They confirmed the presence of two ternary compounds ($CeFe_2Si_2$ and Ce_2FeSi_3) and discovered two new compounds ($CeFeSi_2$ and CeFeSi). A relatively recent study of the Ce-Fe-Si system at 900 °C by Berthebaud et al. [14] revealed two additional compounds of $Ce(Fe_{13-x}Si_x)$ ($2.4 \leq x \leq 2.6$) and $Ce(Fe_{13-y}Si_y)$ ($3.5 \leq y \leq 5$) compositions. They [14] also corrected the composition of Ce_2FeSi_3 compound to be $Ce_5Fe_2Si_8$. Because of the combined use of XRD and SEM/EDS, Berthebaud et al. [14] published more detailed and precise description of the Fe-rich corner and ternary solubilities of binary compounds compared to the work of Bodak et al. [13]. Obviously, the presence of many ternary compounds makes the phase equilibria in this system complex.

The experimental data on Ce-Fe-Ni is limited. This system is characterized by complete solid solution between the $CeFe_2$ and $CeNi_2$ compounds [7,15,16]. Fe substitutes Ni in $CeNi_5$ compound up to $CeFeNi_4$ composition [7,17]. This will be verified in the current work. The ternary phase diagram of Ce-Fe-Ni could not be found in the literature. Therefore, it is necessary to further investigate the Ce-Fe-Ni ternary system, especially because no reports could be found on all the ternary solubilities of the constituent binary compounds except for $CeNi_5$, $CeFe_2$ and $CeNi_2$. This system is studied in this paper.

3. Experimental procedure

The starting materials are Al ingots with purity 99.7 wt.%, B pieces with purity 99.5 wt.%, Ce ingots with purity 99.9 wt.%, Fe pieces with purity 99.99 wt.%, Si lump with purity 99.9999 wt.% and Ni pieces with 99.99 wt.% purity which were all supplied by Alfa Aesar. Arc-melting furnace, equipped with a water-cooled copper crucible and a non-consumable tungsten electrode, was used to prepare the key alloys under argon protective atmosphere and later annealed at 900 °C for 10 days. The samples were quenched in a cold water bath to obtain high-temperature structure. Diffusion couple was prepared by grinding down the contacting surfaces of the end-members to 1200 grit SiC paper and then polishing using 1 μm water-based diamond suspension with 99% pure ethanol as lubricant. The two end-members were carefully pressed against each other, and then clamped with a steel ring. After clamping, the couple is sealed in a quartz tube filled with argon for annealing at 900 °C and periods of 36 and 39 days.

Hitachi S-3400 N Scanning Electron Microscopy (SEM) coupled with Wave-Dispersive X-ray Spectroscopy (WDS) and Energy-Dispersive X-ray Spectroscopy (EDS), XRD, and magnetic force microscopy are used to analyze the diffusion couples and key alloys. The area analysis of SEM/EDS is used to determine the actual compositions of both diffusion couples and key alloys while SEM/WDS has been used to analyze compositions, morphologies and homogeneity ranges of the constituent phases observed in the diffusion couples and key alloys. The estimated measurement error in WDS and EDS is ±2 at.%. XRD is used to determine the available phases, their relative amounts and provides information on the crystal structures of the phases in the key alloys. XRD patterns are obtained using PANanalytical Xpert Pro powder X-ray diffractometer with Cu radiation having 1.5405980 Å K-Alpha 1 and 1.5444260 Å K-Alpha 2 wavelengths at 45 kV and 40 mA from 20 to 90° 2θ with a 0.02° step size. Key alloys with compositions matching the phases observed in the Fe-rich regions of the Ce-Fe-{Ni, Si, Al}-B quaternary systems, are prepared and analyzed with magnetic force microscopy. The parameters used to obtain magnetic force microscopy magnetic micrographs are 30 μm scan size, 1 Hz scan rate, 0.2 integral gain, 0.4 proportional gain, tapping mode and they are kept the same for all the key alloys prepared in the Ce-Fe-{Ni, Si, Al}-B quaternary systems.

4. Results and discussion

This work involves three quaternary systems, namely Ce-Fe-Ni-B, Ce-Fe-Si-B, and Ce-Fe-Al-B. Six solid state diffusion couples and various numbers of key alloys were used to investigate the Ce-Fe-Ni-B and Ce-Fe-Si-B systems. The study of the Ce-Fe-Al-B was performed with key alloy technique only. Both the diffusion couples and key alloys employed in the study of the Ce-Fe-{Ni, Si, Al}-B quaternary systems were annealed at 900 °C. Single phase alloy was difficult to obtain due to the deviation of the actual from the nominal composition, due mainly to evaporation. Hence, the global composition is very close to the composition of the phase of interest, $Ce_2(Fe, M)_{14}B$, indicating that the amount of the other phases is very small.

4.1. Phase equilibria

4.1.1. Ce-Fe-Ni-B quaternary system

Three diffusion couples were used in investigating the Fe-Ni side of the Ce-Fe-Ni-B quaternary system. These diffusion couples were annealed at 900 °C for 39 days and their terminal compositions are: 1: Ce15Fe74B11–Ni75B25, 2: Ce9Fe83B8–Fe31Ni69, and 3: Ce15Fe74B11–Fe31Ni69.

End-member 1 of diffusion couple 1 is an alloy with actual composition of Ce15Fe74B11 at.%. It contains a three-phase equilibrium among $CeFe_2$, $Ce_{1.1}Fe_4B_4$ and $Ce_2Fe_{14}B$, which is consistent with the Ce-Fe-B phase diagram [7]. The end-member 2 is a single-phase alloy of the Ni_3B compound. Eight diffusion zones were observed in this diffusion couple and in general, Ni is diffusing from end-member 2 towards the other end of this couple. The order of the diffusion zones from end-member 1 is deduced as: $CeFe_2 + Ce_{1.1}Fe_4B_4 + Ce_2Fe_{14}B$ (end-member) → $Ce_{1.1}Fe_4B_4 + Ce_2(Fe_{14-x}Ni_x)B$ ($0 \leq x \leq 1.5$) → α-Fe → $Ce(Ni_{3-x}Fe_x)$ ($0 \leq x \leq 1.72$) + α-Fe + $Ce(Ni_{4-x}Fe_x)B$ ($0 \leq x \leq 0.78$) → α-Fe + $Ce(Ni_{4-x}Fe_x)B$ ($0 \leq x \leq 0.78$) + Fe_2B → $Ce(Ni_{4-x}Fe_x)B$ ($0 \leq x \leq 0.78$) + $Ce_2(Ni_{7-x}Fe_x)$ ($0 \leq x \leq 1.14$) → $Ce(Ni_{4-x}Fe_x)B$ ($0 \leq x \leq 0.78$) → $(Fe_{1-x-y}Ni_xCe_y)_{23}B_6$ ($0 \leq y \leq 0.062$) ($x = 0.832$) → Ni_3B (end-member). In the diffusion zone 2, which is next to end-member 1, a quaternary solid solubility of Ni in the $Ce_2Fe_{14}B$ is in equilibrium with the $Ce_{1.1}Fe_4B_4$ compound. The amount of Ni measured in the $Ce_2Fe_{14}B$ in this zone ranges from 0 to 9 at.%. Quaternary solid solubility of Fe in the $CeNi_4B$ was observed in the diffusion zones 4 to 8. The amounts of Fe measured in $CeNi_4B$ are 1–7 at.% and 13–22 at.%, and the observed gap is between 7 at.% Fe and 13 at.% Fe. The last layer is $(Fe, Ni, Ce)_{23}B_6$. In this, Ce substitutes Fe in the $(Fe, Ni)_{23}B_6$ phase between 2 and 5 at.%. Diffusion couples 2 and 3 were prepared to further investigate the Fe-Ni side of the Ce-Fe-Ni-B quaternary systems at 900 °C. Quaternary solubilities of Ni in the $Ce_2Fe_{14}B$ and Fe in the $CeNi_4B$ observed in diffusion couple 1 are also found in diffusion couples 2 and 3.

Six key alloys prepared to further investigate the $Ce_2(Fe_{14-x}Ni_x)B$ at 900 °C for 10 days confirmed the existence of this solid solution. Since the maximum solubility is 9 at.% Ni, the corresponding formula, which represents the amount of measured Ni in this solid solution, is written as $Ce_2(Fe_{14-x}Ni_x)B$ ($0 \leq x \leq 1.5$). XRD analysis of

the $Ce_2(Fe_{14-x}Ni_x)B$ solid solution confirms Ni substitution and shows that the compound crystallizes in tetragonal structure as shown in Table 1. The peak positions shift to higher diffraction angle with decreasing Fe (1.72 Å) content because Ni (1.62 Å) has a smaller atomic radius [18]. The linear relations between lattice parameter c and lattice volume V versus Ni concentration in the $Ce_2(Fe_{14-x}Ni_x)B$ solid solution obey Vegard's law [19] as shown in Fig. 1.

The solubility of Fe in the $CeNi_4B$ compound from the diffusion couples is measured as 1–7 at.% Fe and 13–53 at.% Fe. To further investigate and verify these values, 10 key alloys that were prepared and annealed at 900 °C for 10 days confirm $Ce(Ni_{4-x}Fe_x)B$ solid solution. Out of these 10 key alloys, 3 key alloys were prepared to determine whether the gap observed in the diffusion couples can be confirmed or not, and their compositions were located in the observed gap. Analysis of these three key alloys do not confirm the presence of a gap in the homogeneity range of $Ce(Ni_{4-x}Fe_x)$, because each of these alloys contained a $Ce(Ni_{4-x}Fe_x)B$ solid solution having variable Fe and Ni contents not pointing to fixed composition of the solubility limits. Therefore, it is concluded that $Ce(Ni_{4-x}Fe_x)B$ solid solution is a continuous solid solution and the corresponding formula of this solid solution is written as $Ce(Ni_{4-x}Fe_x)B$ ($0 \le x \le 0.78$) at 900 °C. The occurrence of the $Ce(Ni_{4-x}Fe_x)B$ solid solution is confirmed by XRD analysis and its crystal structure is shown in Table 1. Fe substituting Ni in the $CeNi_4B$ increases lattice parameter, a and lattice volume, V, as shown in Table 2.

Monnier et al. [20] investigated the $(Fe, Ni)_{23}B_6$ compound and confirmed its occurrence with the $Fe_{4.5}Ni_{18.5}B_6$ composition. Stadelmaier et al. [21] reported the $Fe_3Ni_{20}B_6$ composition and stated that it is a metastable compound that solidifies from the melt. However, last diffusion zone of the diffusion couple 1 revealed the $(Fe, Ni)_{23}B_6$ phase which is stabilized by substituting Fe with 2–5 at.% Ce. Therefore, four key alloys were prepared to further investigate $(Fe, Ni, Ce)_{23}B_6$. Concentrations of Ce and Fe were measured in the $(Fe_{1-x-y}Ni_xCe_y)_{23}B_6$ solid solution in these key alloys using SEM/WDS and found ranging from 6 to 12 at.% Fe and 1 to 6 at.% Ce. The results of the key alloys confirms the observation of $(Fe_{1-x-y}Ni_xCe_y)_{23}B_6$ in the diffusion couples. XRD study shows that the varying concentrations of Ce and Fe measured in the $(Fe_{1-x-y}Ni_xCe_y)_{23}B_6$ corresponds to the same crystal structure, which crystallizes in FCC structure with Fm-3m space group as indicated in Table 1. In Table 2, lattice parameters a, b and c are equal and they are increased by the substitution of Fe by Ce in the $(Fe_{1-x}Ni_x)_{23}B_6$. XRD results show that $(Fe_{1-x-y}Ni_xCe_y)_{23}B_6$ is a solid solution which has a wide homogeneity range of Ce between 0 and 6 at.%. Therefore, the corresponding formula of this solid solution at 900 °C is written as $(Fe_{1-x-y}Ni_xCe_y)_{23}B_6$, where $0 \le y \le 0.062$ and $x = 0.832$. Nevertheless, we consider the results pertinent to this solid solution preliminary and due to the complex atomic exchange among

Table 1
Crystal structures of compounds.

S/N	Compound	Structure type	Space group	Prototype
1	$Ce_2Fe_{14}B$ containing Ni, Si, Al	Tetragonal	$P4_2/mnm$	$Nd_2Fe_{14}B$
Ce-Fe-Ni-B system				
2	$Ce(Ni_{4-x}Fe_x)B$	Hexagonal	$P6/mmm$	$CeCo_4B$
3	$(Fe_{1-x-y}Ni_xCe_y)_{23}B_6$	FCC	Fm-3m	$Cr_{23}C_6$
Ce-Fe-Si-B system				
4	$(Fe_{1-x-y}Si_xCe_y)_3B$	Orthorhombic	$Pnma$	Fe_3C
5	$(Fe_{1-x-y}Si_xCe_y)_{23}B_6$	FCC	Fm-3m	$Cr_{23}C_6$

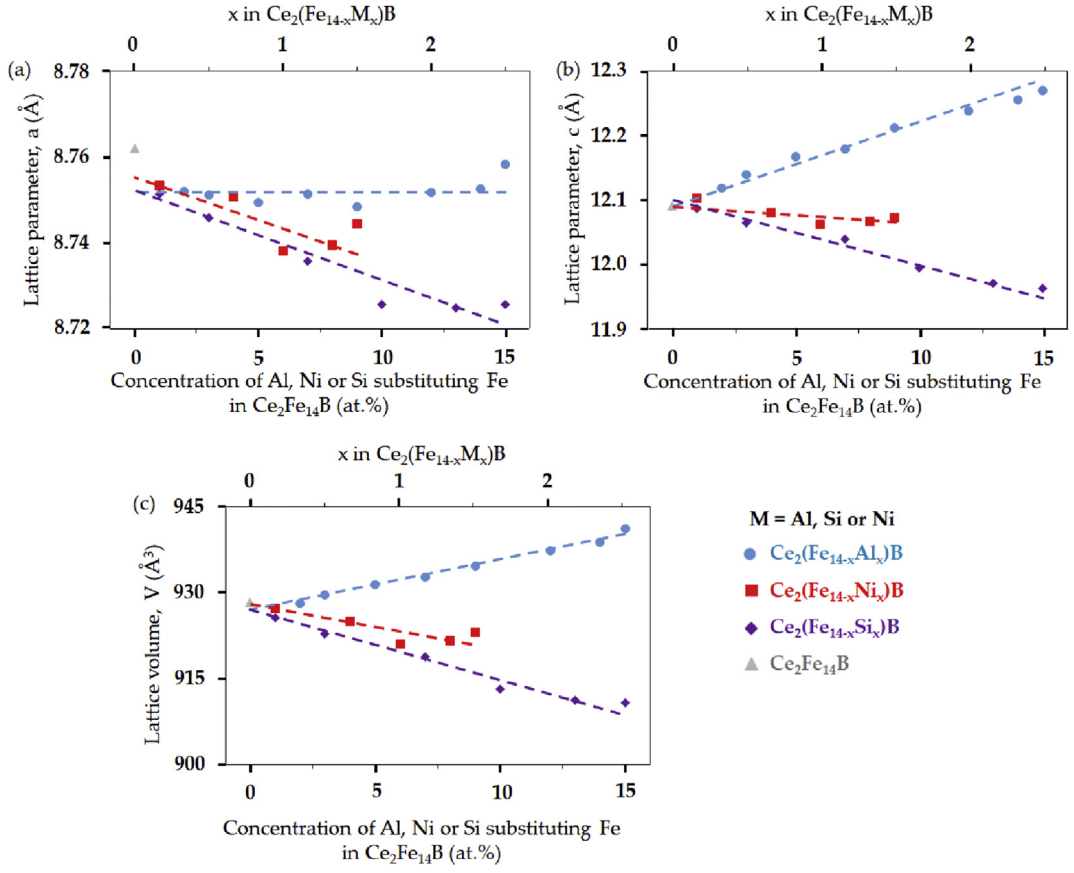

Fig. 1. Effect of Al, Ni, or Si content in the $Ce_2(Fe_{14-x}M_x)B$ compound on the (a) lattice parameter, *a*; (b) lattice parameter, *c*; (c) lattice volume, *V*.

Table 2
Lattice parameters and volumes of quaternary extensions of $CeNi_4B$, $Fe_{23}B_6$ and Fe_3B.

S/N	Compound	Composition (at.%)			Lattice parameter (Å)			Volume V (Å^3)
		Ce	Fe	Ni	a	b	c	
Ce-Fe-Ni-B System								
0	$Ce(Ni_{4-x}Fe_x)B$	15	0	68	5.0050	5.0050	6.9920	175.1498
1		15	4	64	5.0040	5.0040	6.9674	174.4638
2		15	5	63	5.0064	5.0064	6.9688	174.6663
3		15	14	54	5.0172	5.0172	6.9754	175.5868
4		15	24	44	5.0244	5.0244	6.9743	176.0634
5		15	42	26	5.0359	5.0359	6.9787	176.9819
6		15	50	18	5.0417	5.0417	6.9682	177.1229
7		15	53	15	5.0436	5.0436	6.9711	177.3302
0	$(Fe_{1-x-y}Ni_xCe_y)_{23}B_6$	0	40	40	10.6900	10.6900	10.6900	1221.6115
1		2	11	67	10.5195	10.5195	10.5195	1164.0866
		3	9	67				
2		1	12	67	10.5464	10.5464	10.5464	1173.0397
		4	8	67				
3		6	6	67	10.6595	10.6595	10.6595	1211.1851
Ce-Fe-Si-B system								
S/N	Compound	Composition (at.%)			Lattice parameter			Volume V
		Ce	Fe	Si	a	b	c	
0	$(Fe_{1-x-y}Si_xCe_y)_{23}B_6$	0	40	40	10.6900	10.6900	10.6900	1221.6115
1		7	63	8	10.4222	10.4222	10.4222	1132.0828
0	$(Fe_{1-x-y}Si_xCe_y)_3B$	0	68	8	5.4100	6.6000	4.4600	159.2488
1		7	60	8	5.4019	6.5226	4.5162	159.1258

Fe, Ni and Ce, further study using single crystal XRD analysis is recommended. Combining the results of diffusion couples and key alloys, the phase relationships in the Fe-Ni side of the Ce-Fe-Ni-B quaternary system is drawn in Fig. 2.

There are limited experimental data on the Ce-Fe-Ni system and no phase diagram could be found in the literature. Thus, we decided to study it in this work. It was reported that, a ternary solid solubility of Fe in the $CeNi_5$ extends up to the $CeNi_4Fe$ composition and an unlimited solid solution exists between $CeNi_2$ and $CeFe_2$ [7]. In the three diffusion couples discussed above, $Ce_2(Ni, Fe)_7$, $Ce(Ni, Fe)_3$ and $Ce(Ni, Fe)_5$ with the 18–25 at.% Fe, 37–43 at.% Fe and 5–24 at.% Fe compositions were respectively observed. This showed that Ce_2Ni_7 and $CeNi_3$ intermetallics extend into the Ce-Fe-Ni ternary system and that the extension of $CeNi_5$ is more than the $CeNi_4Fe$ composition reported by Refs. [7,15–17]. Based on these observations from diffusion couples, the Fe-Ni side of the Ce-Fe-Ni ternary system is further investigated in this work. Five key alloys were also prepared to further investigate the ternary solid solubilities of Fe in $CeNi_5$, Ce_2Ni_7 and $CeNi_3$ in the Ce-Fe-Ni ternary system. Results of these key alloys confirm that $CeNi_5$, Ce_2Ni_7 and $CeNi_3$ extend into the Ce-Fe-Ni ternary system, confirming what has been observed in the diffusion couples. In this work, the $CeNi_3$ and Ce_2Ni_7 compounds have been confirmed to extend into the Ce-Fe-Ni ternary system. Also, the ternary solid solubility of Fe in the $CeNi_5$, which

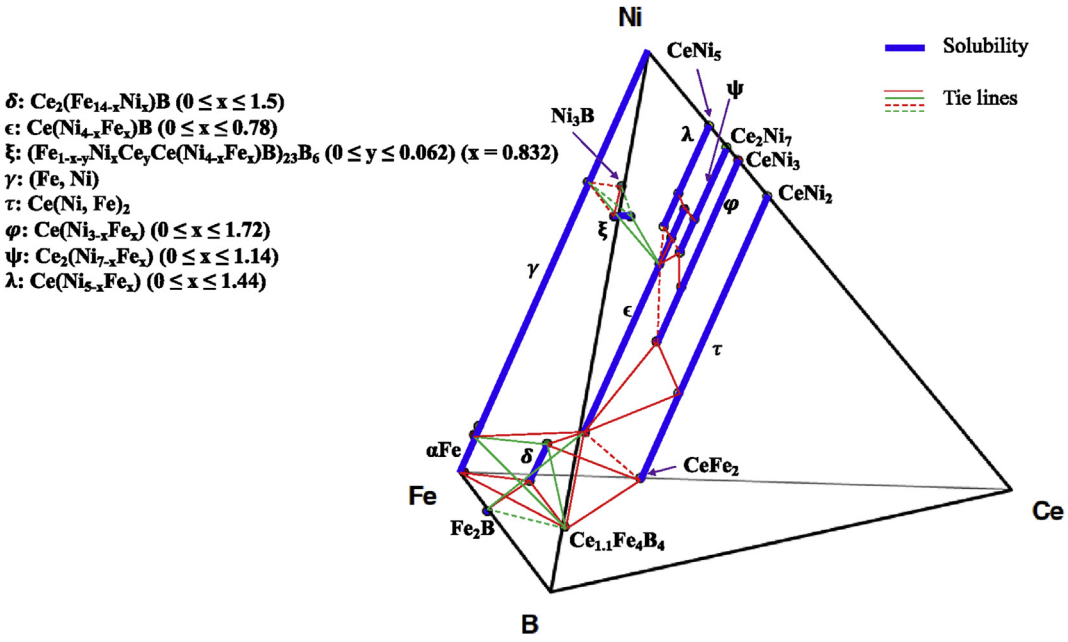

Fig. 2. The phase relationships in the Fe-Ni side of the Ce-Fe-Ni-B quaternary system at 900 °C.

was reported to extend up to the $CeNi_4Fe$ composition [7,17], was observed to extend to 19 at.% Fe which is higher than the 16.7 at.% Fe reported by Refs. [7,17]. Although the exact determination of maximum ternary solid solubilities of Fe in the $CeNi_3$, Ce_2Ni_7 and $CeNi_5$ is not the purpose of this work, it has been confirmed that the ternary solid solubilities of Fe in the $CeNi_3$, Ce_2Ni_7 and $CeNi_5$ compounds extend to at least 41 at.% Fe, 16 at.% Fe and 19 at.% Fe, respectively at 700 °C. The results from the three diffusion couples used in studying the Ce-Fe-Ni-B quaternary system at 900 °C have shown that, the ternary solid solubilities of Fe in the $CeNi_3$, Ce_2Ni_7 and $CeNi_5$ compounds extend to at least 43 at.% Fe, 25 at.% Fe and 24 at.% Fe, respectively. The results from these three sets of diffusion couples are self-supportive as Fe/Ni atomic exchange is expected to increase by increasing the temperature from 700 °C to 900 °C. Based on the experimental results obtained in this work and the literature data, a partial isothermal section of the Ce-Fe-Ni ternary system at 700 °C is drawn in Fig. 3.

4.1.2. Ce-Fe-Si-B quaternary system

Three diffusion couples were used in investigating Fe-Si side of the Ce-Fe-Si-B system. The terminal compositions of these diffusion couples, in at.%, are: 1: Ce15Fe74B11– Fe72Si28, 2: Ce10Fe82B8–Si, and 3: Ce12Fe72B16–Si. End-member 1 of diffusion couple 1 is an alloy of Ce15Fe74B11 composition. It contains a three-phase equilibrium among $Ce_{1.1}Fe_4B_4$, $Ce_2Fe_{14}B$ and $CeFe_2$, which is in accord with the Ce-Fe-B phase diagram [7]. End-member 2 is Fe_3Si single phase. After annealing diffusion couple 1 for 36 days at 900 °C, five diffusion layers were observed and WDS spot analysis was carried out to determine the composition of phases present in these layers. The order of the diffusion layers from end-member 1 is: $Ce_{1.1}Fe_4B_4$ + $CeFe_2$ + $Ce_2Fe_{14}B$ (end-member) → $Ce_{1.1}Fe_4B_4$ + $Ce_2(Fe_{14-x}Si_x)B$ $(0 \le x \le 2.33)$ → $Ce_3(Si_{2-x}Fe_x)$ $(0 \le x \le 0.1)$ → CeFeSi → $CeFe_2Si_2$ → $Ce(Fe_{13-x}Si_x)$ $(3.5 \le x \le 5)$ → Fe_3Si (end-member). $Ce_2(Fe_{14-x}Si_x)B$ contains 0–11 at.% Si in diffusion couple 1. Diffusion zone 3 is $Ce_3(Si_{2-x}Fe_x)$, in which Si is substituted by 1–2 at.% of Fe and a single phase of the $Ce(Fe_{13-x}Si_x)$ with 33 at.% Si is observed in diffusion zone 6.

Diffusion couples 2 and 3 were prepared to further understand the phase relationships in the Fe-rich region of the Ce-Fe-Si-B quaternary system at 900 °C. The results of diffusion couple 3 only confirmed those obtained by the diffusion couple 2 because it followed similar diffusion path. $Ce_2(Fe_{14-x}Si_x)B$ observed in diffusion couple 1 is also observed in diffusion couples 2 and 3.

Based on the experimental results obtained from the three diffusion couples, 8 key alloys were prepared to confirm and further investigate $Ce_2(Fe_{14-x}Si_x)B$. Results obtained from the key alloys have confirmed the solubility of Si in the $Ce_2Fe_{14}B$ compound. Homogeneity range of Si in this compound is determined to be between 0 and 14 at.% Si. The corresponding formula taking into account Si concentration in this solid solution is $Ce_2(Fe_{14-x}Si_x)B$ $(0 \le x \le 2.33)$. XRD analysis confirmed the solid solubility of Si in the $Ce_2Fe_{14}B$ compound and Table 1 shows its crystal structure-type. The substitution of Fe (1.72 Å) by Si (1.46 Å) [18], which has a smaller atomic radius, decreases the unit cell parameters in the $Ce_2Fe_{14}B$ and this is confirmed by the increment of 2θ values of the peak positions and their shift to higher angle. The linear relations of lattice parameter and lattice volume versus Si concentration indicate that $Ce_2(Fe_{14-x}Si_x)B$ obeys Vegard's law [19] as shown in Fig. 1. This is also an indication that substitution solid solubility occurs in the $Ce_2(Fe_{14-x}Si_x)B$.

Results of key alloys 6, 7 and 8 have shown that Fe_3B and $Fe_{23}B_6$ extend into the Ce-Fe-Si-B quaternary system through Ce and Si substitutions for Fe forming solid solutions. These solid solutions are only discussed briefly in this study, because they have no potential for permanent magnet materials. Concentrations of 7 at.% Ce and 8 at.% Si were measured in the $(Fe_{1-x-y}Si_xCe_y)_3B$ $(x = 0.107, y = 0.093)$ phase. Contents of Ce and Si measured in the $Fe_{23}B_6$ are 7 and 8 at.%, respectively. The corresponding formula of this compound is written as $(Fe_{1-x-y}Si_xCe_y)_{23}B_6$, where $x = 0.099$ and $y = 0.087$. The crystal structures and lattice parameters of $(Fe_{1-x-y}Si_xCe_y)_3B$ and $(Fe_{1-x-y}Si_xCe_y)_{23}B_6$ are shown in Tables 1 and 2, respectively. The phase relationships in the Fe-Si side of the Ce-Fe-Si-B quaternary system at 900 °C, obtained through diffusion couples and key alloys, is drawn in Fig. 4.

4.1.3. Ce-Fe-Al-B quaternary system

Key alloy technique has been used in this work to experimentally investigate the quaternary extension of the $Ce_2Fe_{14}B$ compound in the Ce-Fe-Al-B system. Based on the experience from the results of the $Ce_2(Fe, Ni)_{14}B$ and $Ce_2(Fe, Si)_{14}B$ solid solutions, key alloys containing various levels of Fe/Al substitution in the $Ce_2(Fe, Al)_{14}B$ homogeneity range were prepared. Homogeneity range of Al in the $Ce_2(Fe_{14-x}Al_x)B$ solid solution at 900 °C is between 0 and 15 at.% Al. The corresponding formula of this solid solution is $Ce_2(Fe_{14-x}Al_x)B$ $(0 \le x \le 2.5)$ at 900 °C. The phase relationships in the Fe-rich region of the Ce-Fe-Al-B quaternary system at 900 °C, obtained through key alloys, is drawn in Fig. 5.

XRD analysis confirmed the solubility of Al in the $Ce_2(Fe_{14-x}Al_x)B$ solid solution observed in the key alloys by SEM/WDS. The substitution of Fe by Al increases the lattice volume of the $Ce_2Fe_{14}B$. This is confirmed by the decrease of the 2θ values of the peak positions and their shift to lower angle as the Al concentration

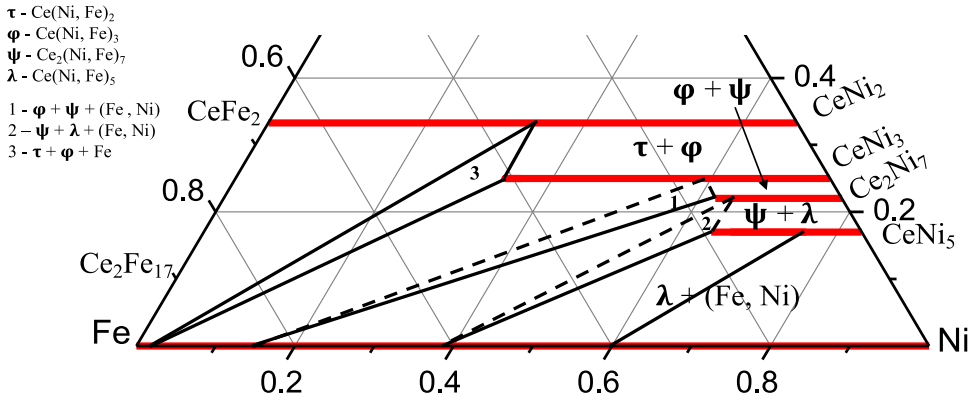

Fig. 3. Partial isothermal section of the Ce-Fe-Ni system at 700 °C.

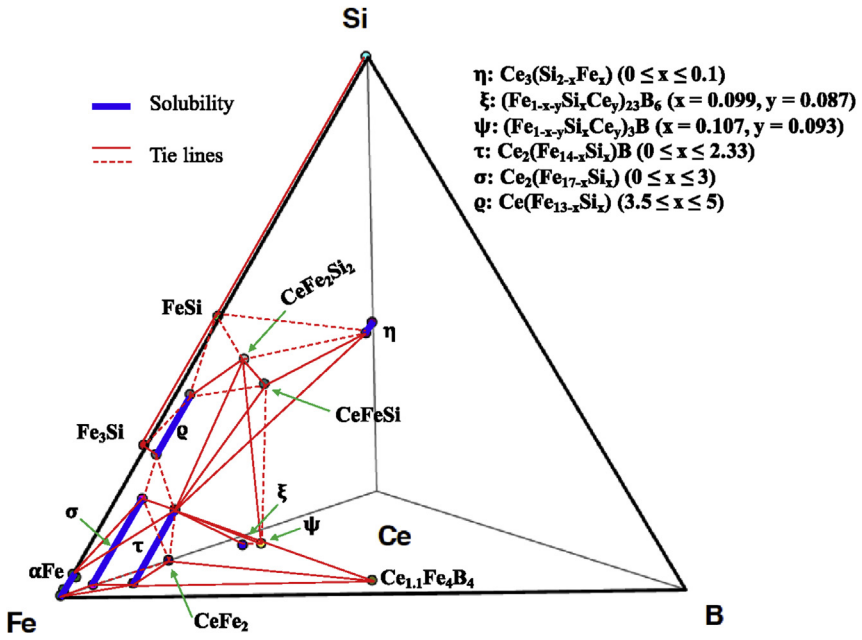

Fig. 4. The phase relationships of the Fe-Si side of Ce-Fe-Si-B quaternary system at 900 °C.

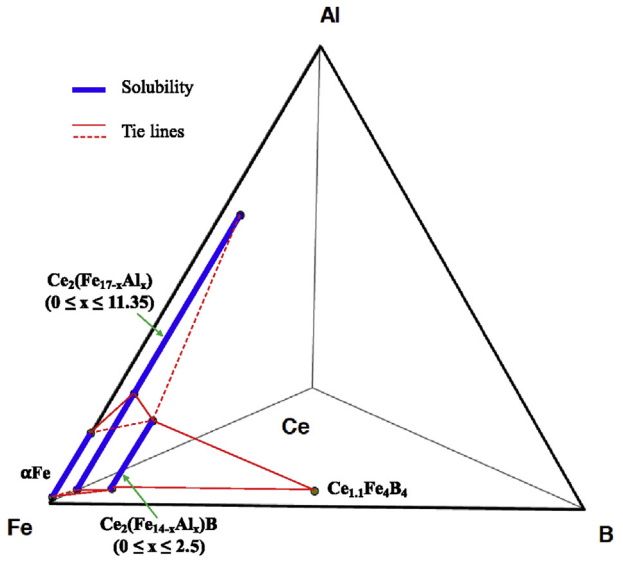

Fig. 5. The phase relationships in the Fe-rich region of the Ce-Fe-Al-B quaternary system at 900 °C.

increases. The linear relations of lattice parameter and lattice volume versus Al concentration in the $Ce_2(Fe_{14-x}Al_x)B$ prove that this solid solution obeys Vegard's law [19] as plotted in Fig. 1. This clearly indicates that substitution solid solubility occurs between Fe and Al in the $Ce_2(Fe_{14-x}Al_x)B$.

4.2. Magnetic force microscopy characterization of phases in the Fe-rich regions of the Ce-Fe-{Ni, Si, Al}-B quaternary systems

The phases observed in the studied systems, using diffusion couples and key alloys, have been tested with magnetic force microscopy. This is to identify the magnetic phases and screen out non-magnetic phases in the Fe-rich regions of the Ce-Fe-{Ni, Si, Al}-B systems. The morphology of magnetic domains can be described as stripe or closure domain [22]. In this work, the domain structures and the magnetic interaction strength of the observed phases in each system are imaged and compared with one another. All magnetic force microscopy micrographs are obtained using the same parameters for easier comparison.

Out of the phases observed in the Fe-rich regions of the three quaternary systems studied in this work, only quaternary solid solution of $Ce_2Fe_{14}B$ containing Ni, Si or Al substituents shows magnetic domain structure of stripe pattern. The strength of the magnetic domain decreases as the concentration of Ni, Si or Al increases along the compositions of the $Ce_2(Fe, M)_{14}B$ solid solution, where M = Ni, Si or Al. Fig. 6(a–c) shows typical magnetic force microscopy micrographs observed for the $Ce_2(Fe, Ni)_{14}B$, $Ce_2(Fe, Si)_{14}B$ and $Ce_2(Fe_{14-x}Al_x)B$ solid solutions. Details of the effects of Ni, Si or Al substituent on the intrinsic magnetic properties of $Ce_2Fe_{14}B$ can be found in Ref. [23].

5. Conclusion

With the aid of the solid-solid diffusion couples and key alloys, experimental investigations of the Fe-rich regions of the Ce-Fe-Ni-B, Ce-Fe-Si-B and Ce-Fe-Al-B quaternary systems have been performed. Equilibrium phase relations in the studied regions were determined. No new quaternary compound was detected, but it was identified that compounds such as: $CeNi_4B$ dissolves Fe, $Fe_{23}B_6$ dissolves Ni, Si and Ce, Fe_3B dissolves Si and Ce, and $Ce_2Fe_{14}B$ dissolves Ni, Si and Al. Homogeneity ranges of quaternary solid solutions of $Ce_2Fe_{14}B$ in the Ce-Fe-{Ni, Si, Al}-B systems were determined as $0 \leq Ni \leq 9$, $0 \leq Si \leq 14$ and $0 \leq Al \leq 15$, in at.%. While studying the Ce-Fe-Ni-B system, the phase relations in the Fe-Ni side of the Ce-Fe-Ni ternary system have been established in this work.

Of the phases observed in the Fe-rich regions of the Ce-Fe-{Ni, Si, Al}-B systems, only $Ce_2(Fe, M)_{14}B$ solid solutions, where M = Ni, Si or Al, are magnetic. Magnetic domains of stripe pattern are observed in these solid solutions and their strength decreases as the concentration of the Ni, Si, Al substituents increases. The magnetic domain structures observed in the $Ce_2(Fe, M)_{14}B$ solid

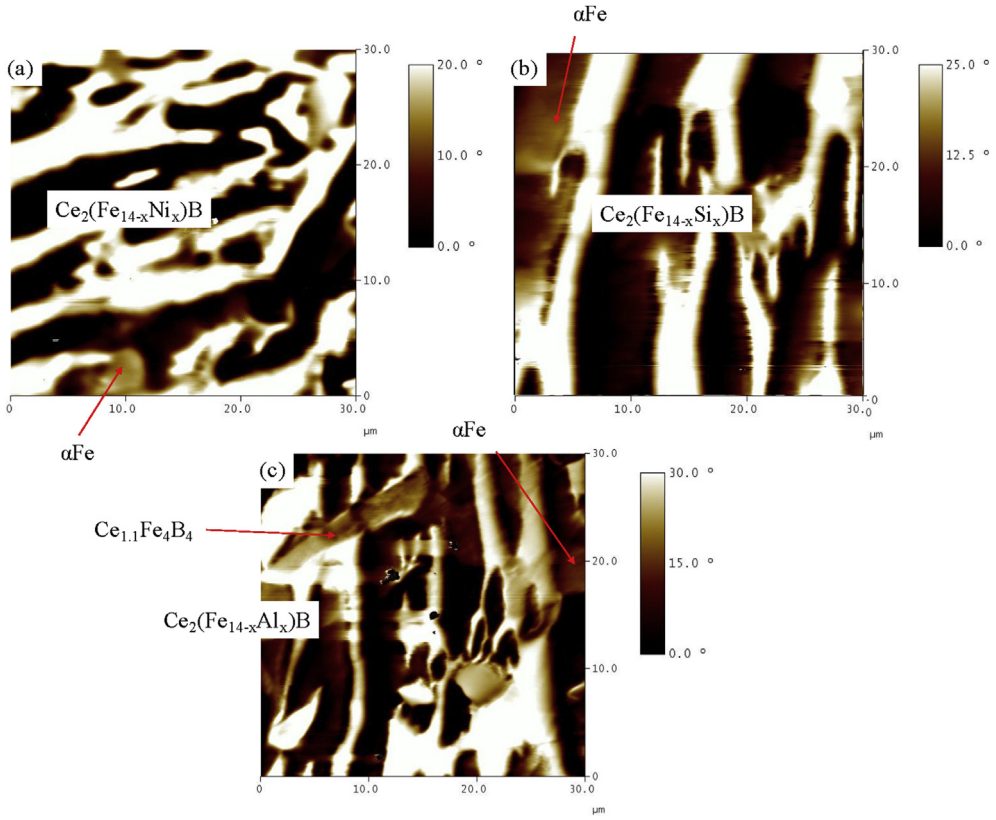

Fig. 6. Typical magnetic force microscopy domain micrographs of the $Ce_2Fe_{14}B$ compound modified by (a) Ni, (b) Si, (c) Al. Scan size of each micrograph is 30 μm.

solutions are indications of the potential of these materials for permanent magnet applications. The intrinsic magnetic properties of the $Ce_2(Fe_{14-x}M_x)B$ solid solutions have been quantified and published in Ref. [23].

Acknowledgement

The authors gratefully acknowledge financial support from NSERC and General Motors (grant number CRD-445897). The authors wish to thank Mr. Tian Wang and members of TMG group for their assistance in carrying out this research.

References

[1] C. Zhou, F.E. Pinkerton, J.F. Herbst, High Curie temperature of Ce–Fe–Si compounds with $ThMn_{12}$ structure, Scr. Mater. 95 (2015) 66–69.
[2] J.F. Herbst, M.S. Meyer, F.E. Pinkerton, Magnetic hardening of $Ce_2Fe_{14}B$, J. Appl. Phys. 111 (7) (2012) 07A718.
[3] H.R. Kirchmayr, Permanent magnets and hard magnetic materials, J. Appl. Phys. 29 (1996) 2763–2778.
[4] N.S. Bilonishko, Y.B. Kuz'ma, The system Ce-Fe-B, Inorg. Mater. 8 (1) (1972) 163–164.
[5] O.M. Dub, N.F. Chaban, Y.B. Kuz'ma, New borides of $Pr_{5-x}Co_{2+x}B_6$-type structure containing iron and cobalt, J. Less Common. Met. 117 (1986) 297–302.
[6] O.M. Dub, Y.B. Kuz'ma, Ternary borides with the $Nd_2Fe_{14}B$ structure, Sov. Powder Metall. Met. Ceram. 25 (7) (1986) 572–575.
[7] V. Raghavan, Phase Diagrams of Ternary Alloys (Monograph Series on alloy Phase Diagram), Part 6A, NRC, 1992.
[8] A. Bezinge, H.F. Braun, J. Muller, K. Yvon, Tetragonal rare earth (R) iron borides, $R_{1+E}Fe_4B_4$ (E=0.1), with incommensurate rare earth and iron substructures, Solid State Commun. 55 (2) (1985) 131–135.
[9] K.L. Meissner, Some examples of the practical use of the clear-cross method, Met. und erz 22 (1925) 243–247.
[10] O.S. Zarechnyuk, M.G. Myskin, V.R. Ryabor, Izv AN SSSR, Izv Akad, Nauk SSSR, Met. 2 (1969) 164–166.
[11] D.F. Franceschini, S.F. da Cunha, Magnetic properties of $Ce(Fe_{1-x}Al_x)_2$ for $x \leq 0.20$, J. Magn. Magn Mater. 51 (1985) 280–290.
[12] V.S. Zolotorevsky, N.A. Belov, M.V. Glazoff, Casting Aluminum Alloys, vol. 1, Elsevier, 2007.
[13] O.I. Bodak, E.I. Gladyshevskii, A.V. Kardash, E.E. Cherkashin, The system cerium-iron-silicon, Inorg. Mater. 6 (6) (1970) 935–938.
[14] D. Berthebaud, O. Tougait, M. Potel, H. Noel, Isothermal section at 900°C of the Ce–Fe–Si ternary system, J. Alloys Compd. 442 (2007) 104–107.
[15] R.C. Mansey, G.V. Raynor, I.R. Harris, Rare-earth intermediate phases. VI. Pseudo-binary systems between cubic laves phases formed by rare-earth metals with iron, cobalt, nickel, aluminium and rhodium, J. Less Common. Met. 14 (1968) 337–347.
[16] I.R. Harris, G. Longworth, X-ray and mossbauer studies of the pseudo-binary system $Ce(Fe_{1-x}Ni_x)_2$, J. Less Common. Met. 45 (1976) 63–77.
[17] H. Oesterreicher, F.T. Parker, M. Misroch, Giant intrinsic magnetic hardness in $RFe_{5-x}Ni_x$ (R=rare earth, x=4 to 5), Appl. Phys. 16 (1978) 185–189.
[18] K. Barbalace, Periodic Table of Elements - Sorted by Atomic Radius, 1995-2018. EnvironmentalChemistry.com, https://environmentalchemistry.com/yogi/periodic/atomicradius.html. (Accessed 13 March 2018).
[19] A.R. Denton, N.W. Ashcroft, Vegard's law, Phys. Rev. A 43 (6) (1991) 3161–3164.
[20] G. Monnier, R. Riviere, M. Ayel, Sur l'existence d'un nouveau compose (Fe, Ni)$_{23}B_6$, borure complexe du type structural $Cr_{23}C_6$, C.R. Acad. Sc. Paris 264 (1967) 1756–1757.
[21] H.H. Stadelmaier, C.B. Pollock, Die metastable tau-phase im system eisen-nickel-bor, Zeitschrift fur Met. 60 (1969) 960–961.
[22] D. Goll, R. Loeffler, J. Herbst, R. Karimi, G. Schneider, High-throughput search for new permanent magnet materials, J. Phys. Condens. Matter 26 (6) (2014) 064208.
[23] K. Orimoloye, D.H. Ryan, F.E. Pinkerton, M. Medraj, Intrinsic magnetic properties of $Ce_2Fe_{14}B$ modified by Al, Ni, or Si, Appl. Sci. 8 (2) (2018) 205.